*Structural Engineering and Mechanics, Vol. 10, No. 5 (2000) 491-504*
DOI: http://dx.doi.org/10.12989/sem.2000.10.5.491


# Inelastic behavior of standard and retrofitted rectangular hollow sectioned struts. I: Analytical model

Medhat K. Boutros†

*The University of Western Australia, Nedlands 6907, Australia*

**Abstract.** This paper is a presentation of a physical model for the elastic-partly plastic behavior of rectangular hollow section pinned struts subjected to static cyclic axial loading and the evaluation of the compressive strength of retrofitted damaged struts. Retrofitting is achieved by welding stiffening plates along the webs of damaged struts. The shape of the elastic and permanent deformations of the strut axis satisfy the conditions at the ends and midspan. Continuous functions of the geometric variables of stress distributions in the yielded zone are evaluated by interpolation between three points along each partly plastic zone. Permanent deformations of the partly plastic region are computed and used to update the shape of the unloaded strut. The necessity of considering geometric nonlinearity is discussed. The sensitivity of the results to the location of interpolation points, the shape of the permanent deformation and material hysteretic properties is investigated.

**Key words:** bracing; compressive strength; cyclic loads; geometric nonlinearity; hysteresis; partial plasticity; retrofitting; steel; struts.

## 1. Introduction

The hysteretic behavior of struts under cyclic loading is an efficient means of energy dissipation in events of excessive dynamic action. Empirical models of their behavior (Jain *et al.* 1978) were developed by piecewise linearisation of experimental observations. In semi-empirical models (Gugerli *et al.* 1982), a plastic hinge was introduced at mid-span and the plastic deformations of the hinge were determined. Analytical solutions using line elements with a perfectly plastic hinge at midspan for pinned struts (Boutros 1991) and at clamped ends (Papadrakakis and Loukakis 1989) exhibited a sudden transition from the elastic condition to the plastic stage due to the instantaneous formation of the plastic hinge that triggered large deflections. They predicted larger compression peaks and midspan deflections than tests (Boutros 1991).

A Finite Strip nonlinear model with a plastic hinge at mid-span (Boutros and Goel 1985) showed the same discrepancies as line element models. It also showed for L sections that the deformation of the cross-section was not large enough to require accounting for distortion of the cross-section and local buckling.

A solution of struts subjected to monotonic loading and including partial plasticity with strain hardening and large deflections (Murray 1991) using numerical integration along the axis of the

† Formerly Lecturer

strut showed a good agreement with test results.

While the assumption of full plasticity at midspan may be appropriate for cases of large plastic strains where axial deformations are larger than five times the yield deformations, practical cases of struts in braced frame structures undergo milder axial deformations (about 2 to 3 times the yield deformations). Therefore, the partly plastic transition stage, where significant portions of the cross-sections about mid-span remain elastic, governs their response. An analytical model where continuous functions of the deformation parameters of the partly plastic zone were derived and explicitly integrated showed a good agreement with test results for circular hollow sections (Boutros 1994).

In this paper, the last model is extended to rectangular hollow sections (RHS). Material hysteretic properties are defined on the basis of test observations (Boutros *et al.* 2000).

The effect of large deflection in the expression of elastic curvature was neglected in most previous analytical studies (Papadrakakis and Loukakis 1989, Boutros 1991). This resulted in errors at large compression deformations when the midspan deflection exceeded 3% of the span as demonstrated below. The axial displacements discussed in this paper and the corresponding tests (Boutros 2000) are generally less than twice the yield axial displacement. These axial displacements correspond to maximum mid-span deflections about 5% of the span length for grade 350 (MPa) steel; which requires accounting for geometric nonlinearity. This model is appropriate for the prediction of the response of bracing members in skeletal structures and of the residual strength of damaged struts. It may also be used to evaluate the shakedown limits of struts for a given loading history.

Following an adverse dynamic loading event on a braced structure, braces may be damaged. Often the extent of damage and/or the difficulty of replacing the braces may justify retrofitting. The model is extended to determine the residual compressive strength of mildly damaged struts after strengthening them with stiffeners, or patches, welded onto their webs.

In the following two sections, the elastic and inelastic relations are presented for both prismatic and retrofitted struts. Then, variations of the model's parameters and assumptions are discussed. Finally, general conclusions are summarised.

## 2. Elastic deformation of the axis

The shape of the elastic curve is shown in Fig. 1. In both the loaded and load-free states, the curvature of the strut is zero at the end pins and the slope is zero at mid-span. The deviation, $v$, from the load axis is defined in terms of straight reference axis $x$, through the ends of the strut, by:

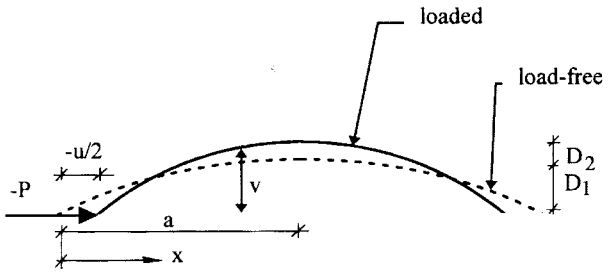


Fig. 1 Deformed shape of the strut axis

$$v_{(x)}=D_1\left(\frac{4x}{3a}-\frac{x^4}{3a^4}\right)+D_2\sin\frac{\pi x}{2a} \qquad \text{for } 0\le x\le a \tag{1}$$

where $D_1$ and $D_2$ are the imperfection and the elastic deflection, respectively, at mid-span and $a$ is the half span of the strut. The permanent imperfection represented by the first term in Eq. (1) varies such that the curvature is quadratic in $x$. The order of the curvature function reflects the extent of the plastic deformations that is mainly dependant on the shape of the cross-section. A solid rectangular cross-section (for which the fully plastic pure bending moment is 50% higher than the yield bending moment) would exhibit a gradual decrease in stiffness along the span from first yield to full plasticity. On the other hand, the stiffness of hollow rectangular sections (for which the difference in magnitudes of the fully plastic and yield bending moments is significantly smaller) will drop steeply once one of its flanges yields. In this case, the plastic deformations would be concentrated in a small midspan yielded zone. In the cases of equal angle cross-sections, a linear variation of the plastic curvature is more adequate (Boutros 1997). The effect of considering a linear curvature is discussed in sub-section 4.2 below.

Axial force $P$ and end displacement $u$ are in the $x$ direction (tension positive) and are shown in Fig. 1 for a positive $D_2$. The relative displacement of the end pins $u_b$ due to bending only was evaluated by equating the lengths of the strut axis in the load-free ($D_2$=0) and loaded ($D_2\neq 0$) configurations:

$$u_b=2a\left(\frac{\Psi}{\Phi}-1\right) \tag{2}$$

where (for small variations of $a$):

$$\Phi=\int_0^a\sqrt{1+v'^2_{(D_1,D_2,x)}}dx \qquad \text{and} \qquad \Psi=\int_0^a\sqrt{1+v'^2_{(D_1,D_2=0,x)}}dx \tag{2a}$$

The total relative displacement of the end pins $u$ is determined by adding the elastic and inelastic axial deflections to the bending one:

$$u=2\left[a\left(\frac{P}{EA}+\frac{\Psi}{\Phi}\right)-a_o\right] \tag{3}$$

where $a_o$ is the initial half span of the strut, a is its current value.

The equilibrium condition due to bending was derived from the stationary of the total energy $\Pi$

$$\Pi=\oint\frac{EI}{2}\phi_e^2dx-Pu_b \tag{4}$$

where $\phi_e$ is the elastic curvature. The curvature was expressed considering the slope of the beam (Timoshenko 1965). The effect of neglecting the slope is discussed in sub-section 4.1 below.

## 3. Inelastic actions and deformations

After initiation of yield, the stress distribution on a cross-section may assume any of three configurations (Fig. 2). First, yield develops in the extreme fibre on the concave face of the strut

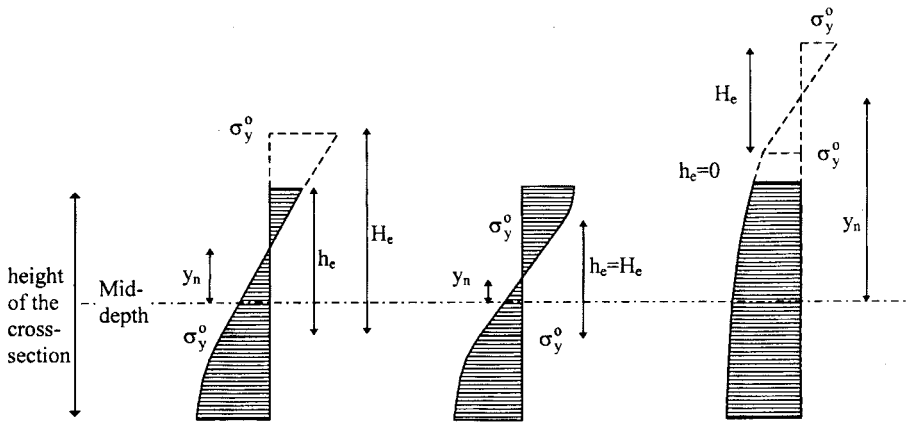


Fig. 2 Inelastic stress distributions on the cross-sections

(bottom fibre in Fig. 2a). In a compression stroke, the yield region spreads inwards while tension stresses increase on the convex face until it yields (top fibre in Fig. 2b). During a tension stroke, the axis of the strut straightens. The stress on the convex face progresses from compression to tension. The yield zone spreads from the concave face to the convex face until the section is fully yielded (Fig. 2c). In Fig. 2, $y_n$ is the position of the neutral axis from mid-height, $h_e$ (real elastic height) is the height of the elastic region of the cross-section and $H_e$ (virtual elastic height) is the height between two points stressed at the nominal yield stress of the material $\sigma_y^o$.

Three key hysteretic stress values are used to describe the plastic history of a cross-section. These are the stress at the extreme fibre on the concave face $\sigma_v$, the stress at the extreme fibre on the convex face $\sigma_x$ and the extreme stress in the elastic portion $\sigma_y^o$. The first two are determined from the plastic strain history. The third is considered to remain constant throughout the analysis.

In the yielded region of any cross-section, the stress distribution is nonlinear. It varies from $\sigma_y^o$ to $\sigma_v$ on the concave side and from $\sigma_y^o$ to $\sigma_x$ on the convex side. The stresses at different fibres follow different histories. Hence, it is difficult to account for the actual stress distribution without complicating the solution significantly. During cyclic loading, the current yield stress at the limits of the elastic zone of the cross-section is different from $\sigma_y^o$ if they have previously yielded. However, it is closer to the nominal value than the yield stress of the extreme fibres because they undergo smaller plastic deformations. At the inner edge of the yielded zone (Fig. 3a), the stress distribution is tangential to that in the elastic zone resulting in a smooth transition between the current (hysteretic) yield stress $\sigma_y^c$ to nominal yield stress $\sigma_y^o$. Then, the error due to assuming this stress to be $\sigma_y^o$ is small.

For simplicity, the stress distribution in each of the concave and convex regions (Fig. 3a) was linearised. Because the only parameters registering the plasticity history are the stress magnitudes at the extreme fibres, it is reasonable to assume that the shape of the equivalent trapezoidal stress block is strongly dependant on the difference between $\sigma_y^o$ and $\sigma_v$ on the concave plastic side (and that between $\sigma_y^o$ and $\sigma_x$ on the convex side) and on the difference between the current yield and ultimate stresses. The latter effect results from the fact that the transition from yield to ultimate stresses is associated with a larger strain variation the larger the difference between these stresses

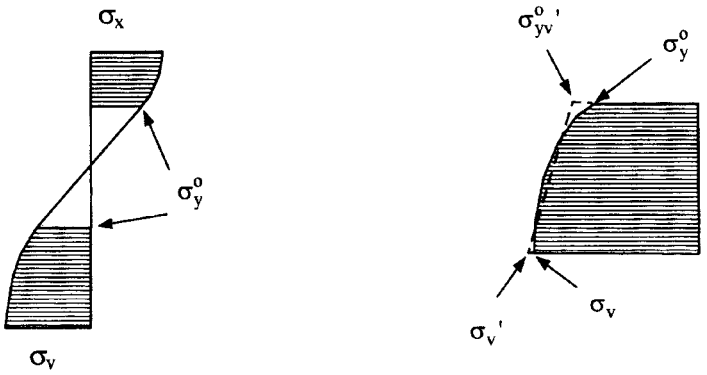


(a) Stress distribution on the cross-section (b) Linearised stresses on the concave side

Fig. 3 Linearisation of the stress distribution in the yielded region

(Boutros *et al.* 2000). On the concave side, the values of $\sigma_y^{o\prime}$ and $\sigma_v'$ (Fig. 3b) were taken as:

$$\sigma_{yv}^{o\prime}=\sigma_y^o+\frac{\sigma_v-\sigma_y^c}{2(\sigma_u^o-\sigma_y^c)}(\sigma_v-\sigma_y^o) \tag{5}$$

and

$$\sigma_v'=\sigma_v+\frac{\sigma_{yv}^{o\prime}-\sigma_y^o}{6} \tag{6}$$

where $\sigma_u^o$, nominal ultimate stress, is defined as the end of the initial curvilinear inelastic stress-strain relation and the beginning of a straight one. Similar relations were used for $\sigma_{yx}^{o\prime}$ and $\sigma_x'$ on the convex side.

In each of the original and patched zones a partly plastic zone may form. Along each partly plastic zone, the stress configuration was determined at three points and the values of the $y_n$ and $H_e$ were determined (Fig. 4, where subscripts *us* and *s* designate the unstiffened and stiffened regions respectively). This was achieved at each point by equating the stress resultants, axial force and bending moment, to the eccentric load $P$ acting at $v$ from the cross-sections midheight. Then, a quadratic function was defined for the variations of $y_n$ and $H_e$.

For a partly plastic segment AB (Fig. 5), the permanent rotation $\delta\theta$, offset $\delta DD$ and axial deformation $\delta_a$ are determined by:

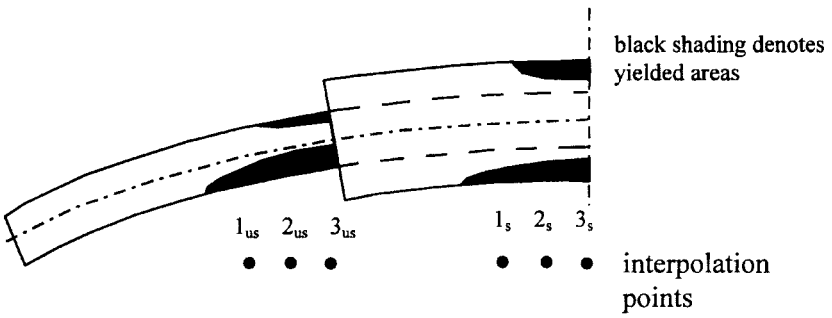


Fig. 4 Interpolation points in the partly plastic zones

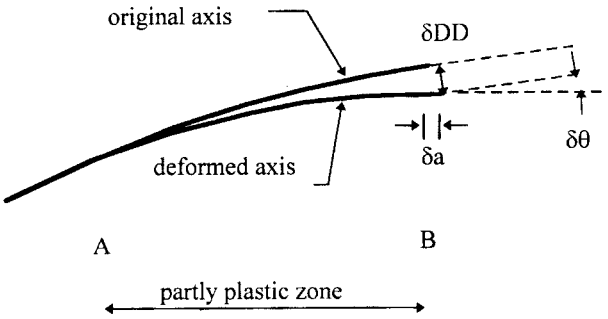


Fig. 5 Deformations of a partly plastic zone

$$\delta\theta=\int_A^B (\phi-\phi_e)dx \tag{7}$$

where $\phi$ and $\phi_e$ are the total and elastic (recoverable upon unloading) curvatures respectively:

$$\phi=\frac{2\varepsilon_y^o}{H_e} \quad \text{and} \quad \phi_e=\left|\frac{Pv}{EI}\right| \tag{7a}$$

$$\delta DD=\int_A^B \int_A^s (\phi-\phi_e)dx\,ds \tag{8}$$

$$\delta a=2\varepsilon_y^o\int_A^B \frac{y_n}{H_e}dx-\frac{|P|}{EA}\int_A^B dx \tag{9}$$

The midspan offset $DD$ due to the permanent deformation of the standard and stiffened regions and the corresponding $D_1$ (Fig. 6) are determined from geometry:

$$DD=DD_o+\delta DD_{us}+L_s\tan(\delta\theta_{us})+\delta DD_s\sec(\delta\theta_{us})=\frac{D_1}{3\sqrt{1+\left(\frac{4D_1}{3a}\right)^2}} \tag{10}$$

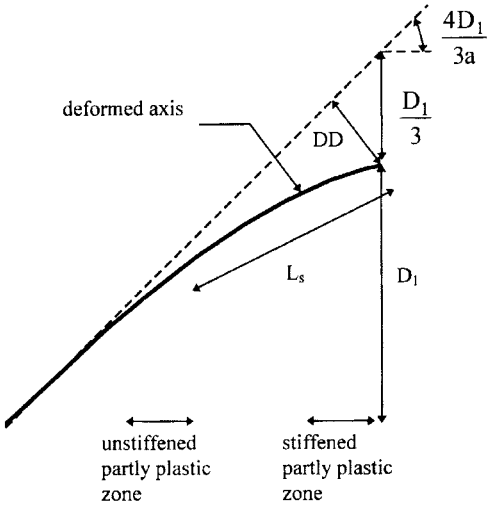


Fig. 6 Permanent deformation of the axis

where $DD_o$ is the original offset and $L_s$ is the half stiffened length of the strut.

In the elastic stage, the analysis was controlled by incrementing the elastic displacement $D_2$. After the onset of yield, it was controlled by decreasing $h_e$ at the most stressed cross-section in the unstiffened zone. When this cross-section was fully yielded, it was controlled by increasing the strain on the convex face.

At the end of each loading stroke of an unstiffened strut, the yield stresses at the concave face for the subsequent stroke were evaluated at the interpolation points of the last step of the stroke and at the pin. A cubic function was derived to fit these four values. This function was used to determine the yield stress on the concave face at any point in the following stroke. On the convex face, isotropic hardening was assumed for simplicity because the inelastic strains on this face are significantly smaller than those on the concave face. Therefore, the hysteretic variations of the yield stress at this fibre are neglected.

In the analysis, a continuous function of the permanent deflection was considered. Plastic deformations of stiffened struts occurred in both their unstiffened and stiffened regions. It usually initiated in the unstiffened regions. Therefore, the expression of the variation of the permanent deformation used in the analysis of unstiffened struts (Eq. 1) was modified to reflect this more uniform spread of permanent curvature along the span by using a lower order (linear) variation of the curvature:

$$v_{(x)}=D_1\left(\frac{3x}{2a}-\frac{x^3}{2a^3}\right)+D_2\sin\frac{\pi x}{2a} \qquad \text{for } 0\le x\le a \tag{11}$$

Eq. 10 and Fig. 6 were modified accordingly.

## 4. Effects of variations in the model's parameters

Few simplifications were introduced in this model namely: the order of the expression of the permanent (plastic) curvature, the locations of interpolation points for the evaluation of plastic deformations and the material hardening path. On the other hand, the commonly assumed small deflection approximation was found inadequate for the practical range of application of this analysis. In this section, these assumptions are discussed and the effects of their variations on the results of the analysis are assessed.

### *4.1. Large versus small deflection elastic curvature*

The expression of the elastic curvature $\phi_e$ in Eq. (6) was derived accounting for the slope of the axis (Timoshenko 1965), i.e.,

$$\phi_e=\frac{v''_{(D_1=0,D_2,x)}}{\left(1+v'^2_{(D_1,D_2,x)}\right)^{3/2}} \tag{12}$$

For small deflections, the denominator approaches unity. The analyses of an elastic compression stroke of a 3.5 m long RHS 65×35×3 strut (slenderness ratio of 248) with an initial imperfection $D_1$ of 50 mm considering the slope in Eq. (12) and neglecting it is shown in Fig. 7. The transverse deflection in the small deflection analysis exhibits stiffening at large deflections due to the

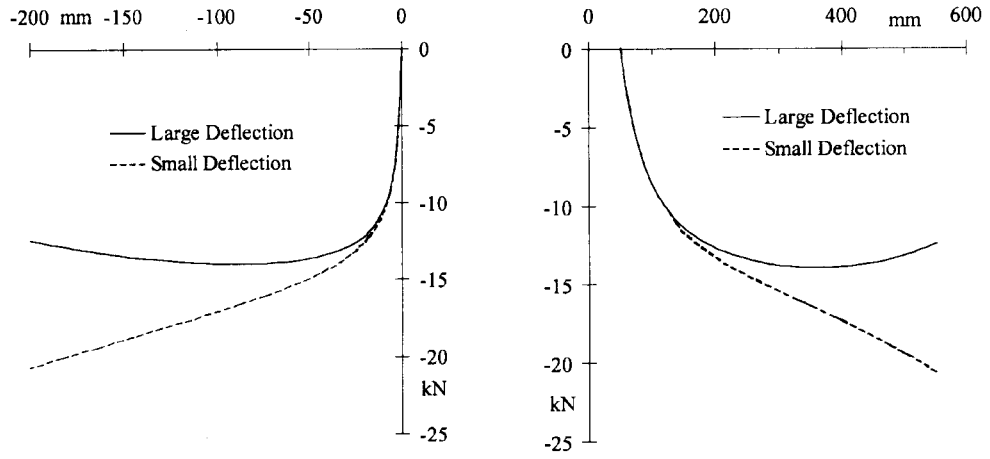


(a) axial load versus axial displacement (b) axial load versus transverse deflection

Fig. 7 Comparison of large and small deflection formulations for a long elastic RHS 65×35×3

shortening of the span which was considered in both analyses. Large deflection formulation is necessary for cases of midspan deflections larger than 3% of the span which is the case for the last quarters of the compression strokes in the cases presented in the experimental study (Boutros *et al.* 2000).

Although the large deflection formulation in Fig. 7 is more accurate than the small deflection one, it is not exact because the sine function of the deflection shape does not satisfy the differential equation for compression forces (negative $P$):

$$EI\frac{v''}{(1+v'^2)^{3/2}}-Pv=0 \tag{13}$$

It is understood that for tension forces the sine function satisfies only the boundary conditions. Equilibrium (Eq. 13) is not satisfied along the span. The error in both tension and compression is however minimised by determining the configuration of stationary total energy (Eq. 4).

### *4.2. Expression of the permanent deflection*

In the analyses above, the expression of the permanent deflection, first term in Eq. (1), corresponded to a quadratic function for the permanent curvature. This choice was substantiated by the shape of the cross-section. For RHS struts, the stiffness of the cross-section is governed by that of its flanges. For an elastic-perfectly plastic material, the fully plastic bending moment and the yield moment of the RHS cross-section are almost equal, whereas the plastic moment of a solid rectangular section is 50% higher than the yield moment. This means that the partly plastic zone would be shorter in the case of RHS than that of the solid cross-section.

Fig. 8 shows the analytical results for an RHS 65×35×3 (test 2 in Boutros *et al.* 2000) with quadratic (Eq. 4) and linear (Eq. 11) expressions for the permanent curvature compared to the experimental results for two cycles of loading. For the same midspan value of $D_1$, the quadratic curvature is associated with smaller load eccentricities away from midspan than the linear case. This

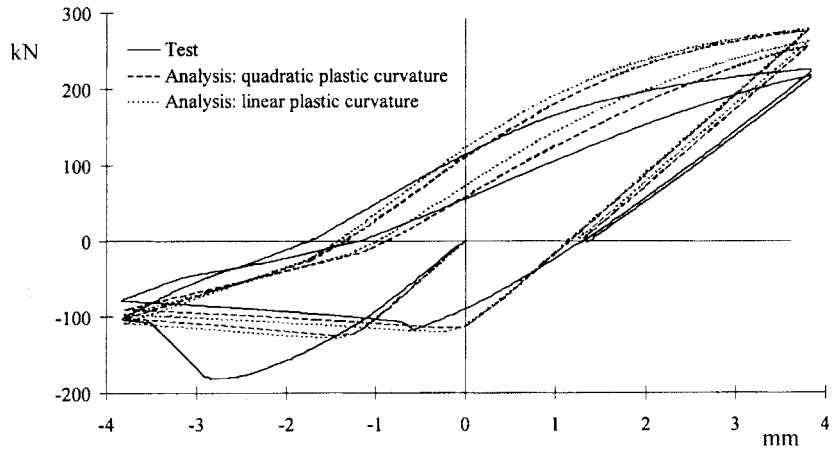


(a) axial load versus axial displacement

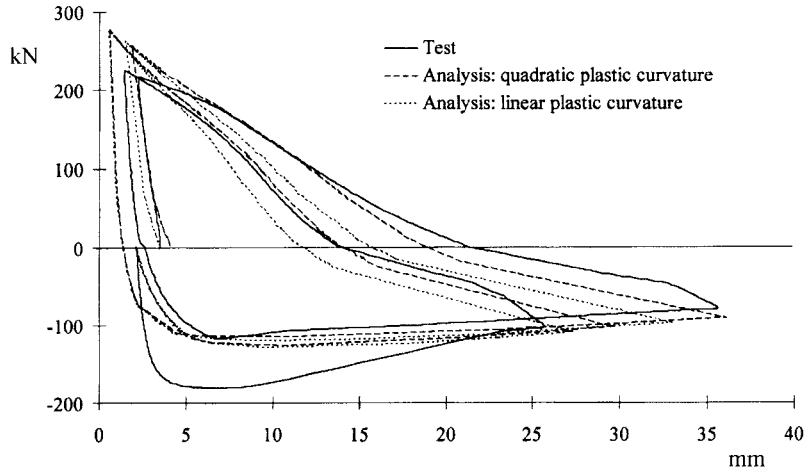


(b) axial load versus transverse deflection

Fig. 8 Comparison of analyses using different distributions of plastic deformations and test (Boutros *et al.* 2000) for RHS 65×35×3

results in larger plastic deformations being required in the case of quadratic curvature to reach the limit axial deformations of the strokes (Fig. 8b). At the end of the tension strokes when $D_1$ is small, especially the first one, the two analyses seem to converge. In general, the analysis with quadratic permanent deformation correlates better with test observations. In the analysis of stiffened struts, it is more adequate to assume a linear permanent curvature because yielding initiates at the ends of the unstiffened zones rather than at midspan.

### 4.3. Location of interpolation points

In each partly plastic zone (Fig. 4), $H_e$ and $y_n$ were evaluated at three points: the most stressed point and two others within the zone. Then, quadratic functions were fitted to these values. The locations of the two intermediate points should be chosen to produce a good global representation of the progress of plastic deformations. In compression where bending plastic deformations are

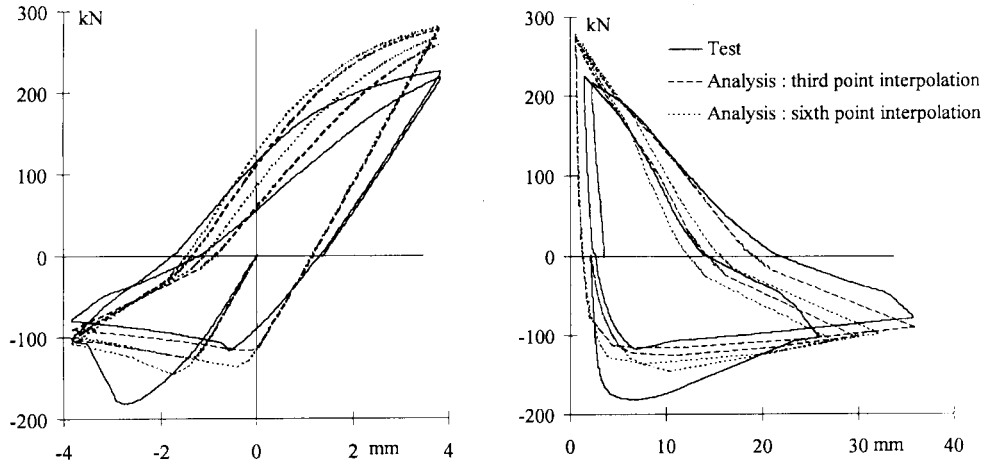


(a) axial load versus axial displacement (b) axial load versus transverse deflection

Fig. 9 Comparison of analysis varying the locations of interpolation points along the partly plastic zone and test (Boutros *et al.* 2000) for RHS 65×35×3

more prominent than axial deformations, these points are better located closer to midspan in order to reflect its prominence for plastic bending deformations. On the other hand, in tension where axial plastic deformations are more important specially after straightening of the strut axis, it is appropriate to spread these points away from midspan. In the cyclic analysis of the unstiffened struts, the intermediate interpolation points were taken at the third points in compression and at the quarter points in tension.

Fig. 9 shows for the second cyclic test the results of two analyses the first using third points for both compression and tension strokes and the other using sixth points (measured from both ends of the half partly plastic zone). In general, the sixth point analysis produces higher load values and smaller permanent deflections than the third point one specially in compression. Also, after the initial friction peak, test and third point analysis converge. However, by varying the locations of the intermediate points between tension and compression, a better agreement with test results is achieved (Boutros *et al.* 2000).

The fact that there are differences in results using third and sixth points means that the assumption of quadratic variations of $H_e$ and $y_n$ is not correct. However, it is convenient in order to simplify the evaluation of plastic deformations in Eqs. (7), (8) and (9). A drawback of this simplification is that the analysis may become unstable if non-positive values of the interpolation function for $H_e$ exist within the partly plastic zone. This instability may be overcome by moving one intermediate point closer to midspan.

A more accurate analysis may be achieved by finite difference integration of the elastic and plastic deformations as presented by Murray (1991) which does not require assuming functions the shape of the axis and the variations of $H_e$ and $y_n$. However, it may be impractical for analysis under cyclic loading. Alternatively, plastic deformations may be evaluated for finite subdivisions of the partly plastic zone. This solution showed to be stable. However, it did not alter the results significantly enough to justify using it in this analysis as the solution process became slower because it required evaluating the stress conditions at 9 or 17 points (for 8 and 16 subdivisions respectively) instead of 3 points in this analysis.

### *4.4. Isotropic versus quasi-kinematic hardening*

Axial tests on full RHS sections (Boutros *et al.* 2000) showed that the hysteretic stress variations were such that the yield stress $\sigma_y^c$ was affected by cyclic loading whereas the ultimate stress $\sigma_u^o$ remained unchanged as shown in the "quasi-kinematic" hardening curve in Fig. 10. Also, the lower the yield stress $\sigma_y^c$ the larger the strain increment between yield and ultimate stresses.

Fig. 11 shows the response considering quasi-kinematic hardening as discussed above and isotropic hardening. It shows that, after the common first stroke, isotropic hardening overestimates stresses up till the end of the strokes. In general, the response using quasi-kinematic hardening is in closer agreement with experiment results in later cycles. Hence, it is important to consider the hardening history of the material. In most cases of stiffened struts, yield initiates at the span end of the unstiffened zone. During the damage event prior to stiffening, this cross-section would incur

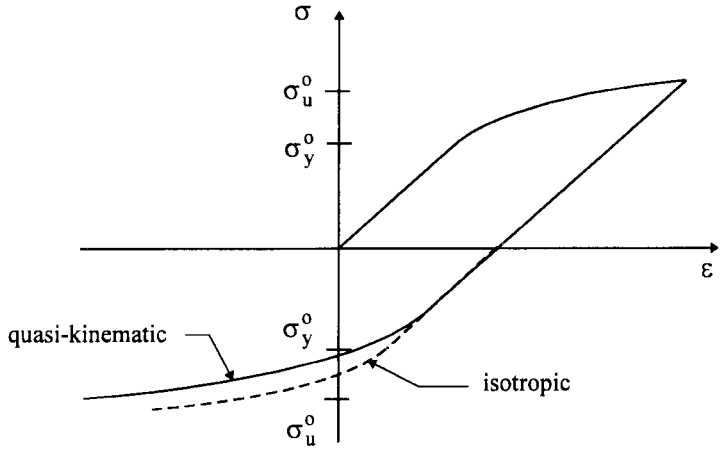


Fig. 10 Hardening paths

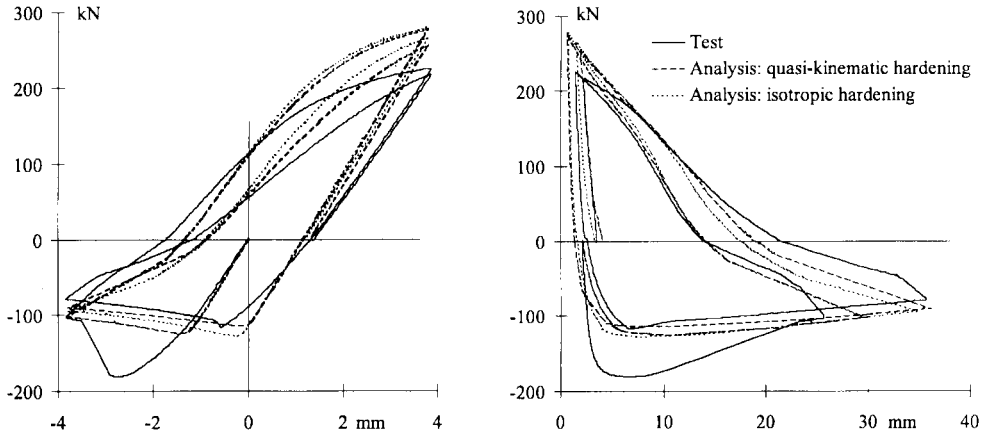


(a) axial load versus axial displacement (b) axial load versus transverse deflection

Fig. 11 Comparison of responses using quasi-kinematic and isotropic hardening and tests (Boutros *et al.* 2000) for RHS 65×35×3

smaller plastic deformations than midspan. Hence, its $\sigma_y^c$ is closer to $\sigma_y^o$. In some cases, compressive strength may depend on yielding of the stiffeners which were not stressed prior to stiffening. At midspan, the yield stress of extreme fibre of the RHS is generally smaller than that of the stiffener. Yet, the stiffener would yield first because of its depth being larger than the RHS. Therefore, the loading history of the original strut may be neglected without significantly reducing the reliability of the analysis.

## 5. Conclusions

A physical model for the elastic-partly plastic behavior of rectangular hollow steel struts subjected to static cyclic axial loading was developed. It was extended to analyse non-prismatic struts for the evaluation of the compressive strength of retrofitted crooked struts. Retrofitting was achieved by welding stiffening plates along the webs of damaged struts. The shape of the elastic and permanent deformations of the axis of the strut satisfied the boundary conditions. The variation of parameters of partial plastic deformations were determined by interpolation between three points along each partly plastic zone. Variations of the analytical model showed that these quadratic functions were an adequate simplification; and that the results were sensitive to the material hysteresis properties. The permanent deformations of the partly plastic region were computed and used to update the shape of the unloaded strut. The shape of the permanent deflections was assumed on the basis of the properties of the cross-section to have a quadratic curvature for the prismatic struts and a linear curvature for the stiffened struts. It was also shown that a large deflection analysis was necessary for struts undergoing midspan deflections larger than 3% of the span.

## References

Boutros, M.K. and Goel, S.C. (1985), "Analytical modelling of braced steel structures" Rep. No. UMCE 85-7, Department of Civil Engineering, The University of Michigan, Ann Arbor, Michigan.

Boutros, M.K. (1991), "Nonlinear SDOF element for hysteretic analysis of pinned bracing members." *J. Engrg. Mechanics, ASCE*, **117**(5), 941-953.

Boutros, M.K. (1994), "Cyclic behaviour of pinned tubes" *Proc., 6th International Symposium on Tubular Structures*, Melbourne, Australia, in Tubular Structures VI, Grundy P., Holgate A. and Wong B, ed., Balkema, Rotterdam, 483-488.

Boutros, M.K. (1997), "Strength of patch-restored crooked pinned L braces." *Proc., International Conference on Rehabilitation and Development of Civil Engineering Infrastructure Systems*, American University in Beirut, Beirut, Lebanon, 555-565.

Boutros, M., McCulloch, J. and Scott, D. (2000), "Inelastic behavior of standard and retrofitted rectangular hollow sectioned struts. II: Experimental study", *Structural Engineering and Mechanics, An Int. J.* **10**(5), 505-516.

Gugerli, H. and Goel, S.C. (1982), "Inelastic cyclic behavior of steel bracing members." Rep. No. UMEE-82R1, Department of Civil Engineering,University of Michigan, Ann Arbor, Michigan.

Jain, A.K., Goel, S.C. and Hanson R.D. (1978), "Hysteresis behavior of bracing members and seismic response of braced frames with different proportions." Rep. No. UMEE 78R3, Department of Civil Engineering, The University of Michigan, Ann Arbor, Michigan.

Murray, N.W. (1991), "The Buckling of a Pin-ended Column of Rectangular Cross-section and Strain Hardening Mild Steel into the Large-deflection Range" *Thin-Walled Structures,* **13**, 85-114.

Papadrakakis, M. and Loukakis, K. (1989), "*Inelastic Cyclic Response of Restrained Imperfect Columns*", *J.*

*Engrg. Mechanics, ASCE*, **114**(2), 295-313.
Timoshenko, S. (1965), *Strength of Materials, Part 1*, Van Nostrand East West Press, 139.

## Notation

| | |
|---|---|
| $A$ | area of the cross-section of the tube |
| $a$ | half span of the strut |
| $DD$ | offset at mid-span from the tangent at the end of the load-free strut |
| $D_1$ | crookedness at mid-span |
| $D_2$ | elastic deflection at mid-span |
| $E$ | modulus of elasticity |
| $h_e$ | height of the elastic region of the section |
| $H_e$ | height of a virtual region of the section between two lines stressed by $\sigma_y^o$ |
| $I$ | second moment of area of the cross-section of the tube |
| $L_s$ | half length of the stiffened region measured along the axis of the deflected strut |
| $P$ | axial force (positive for tension) |
| $u$ | half the relative (axial) displacement of the pins |
| $v$ | deviation of the axis of the strut from the load line |
| $x$ | coordinate axis along the straight load line |
| $y_n$ | location of the neutral axis measured from the centre of the tube |
| $\delta$ | variation |
| $\varepsilon$ | strain |
| $\varepsilon_r$ | reference strain |
| $\varepsilon_y^o$ | initial (nominal) yield strain |
| $\varepsilon_y^c$ | incremental yield strain of the current stroke |
| $\theta$ | slope of the strut axis |
| $\varphi$ | curvature of the strut axis |
| $\varphi_e$ | elastic curvature of the strut axis |
| $\sigma$ | stress |
| $\sigma_y^o$ | initial (nominal) yield stress |
| $\sigma_u^o$ | nominal ultimate stress |
| $\sigma_y^c$ | yield stress at the start of the current yield stage |
| $\sigma_v$ | stress on the concave face |
| $\sigma_v'$ | linearised stress at the concave face |
| $\sigma_{yv}^{o\prime}$ | linearised yield stress on the concave side |
| $\sigma_x$ | stress on the convex face |
| $\sigma_x'$ | linearised stress at the convex face |
| $\sigma_{yx}^{o\prime}$ | linearised yield stress on the convex side |

### Superscripts

| | |
|---|---|
| $o$ | initial (nominal) value |
| $c$ | current value |

### Subscripts

| | |
|---|---|
| $b$ | bending |
| $e$ | elastic |
| $n$ | neutral axis |
| $r$ | reference |
| $s$ | stiffened region |
| $u$ | ultimate |

| | |
|---|---|
| *us* | unstiffened region |
| *v* | concave face |
| *x* | convex face |
| *y* | yield |